Regularized Iterative Image Restoration with Ringing Reduction

REGINALD L. LAGENDIJK, STUDENT MEMBER, IEEE, JAN BIEMOND, SENIOR MEMBER, IEEE, AND DICK E. BOEKEE

Abstract—**Linear space-invariant image restoration algorithms often introduce ringing effects near sharp intensity transitions. In this paper, it is shown that these artifacts are attributable to the regularization of the ill-posed image restoration problem. Two possible methods to reduce the ringing effects in restored images are proposed. The first method incorporates deterministic *a priori* knowledge about the original image into the restoration algorithm. The second method locally regulates the severity of the noise magnification and the ringing phenomenon, depending on the edge information in the image. A regularized iterative image restoration algorithm is proposed in which both ringing reduction methods are included by making use of the theory of the projections onto convex sets and the concept of norms in a weighted Hilbert space.**

Both the numerical performance and the visual evaluation of the results obtained by the proposed restoration technique are significantly more favorable than the results obtained by linear space-invariant restoration filters without the two ringing reduction methods.

I. Introduction

In image restoration, the ultimate goal is to recover the original scene from a degraded version. The image degradations may be due to a relative motion between the camera and the original scene, defocusing of the lens system, or atmospheric turbulence, and may often be modeled by a linear blur. In addition, the blurred image is nearly always corrupted by an additive random noise term, originating, for example, from the recording medium (film grain noise), discretization of the data, or measurements errors. The noisy blurred image can then be described by the following algebraic model [1]:

$$g = Df + n, \tag{1}$$

where the linear distortion operator D is known or can be satisfactorily identified [2], [3]. The original and noisy blurred images are denoted by the lexicographically ordered vectors f and g, respectively. The additive term n represents the noise, which is uncorrelated with the image f.

Since n is a realization of a stochastic process, its characteristics are only partially known in practice. As a consequence, the exact original image f cannot be computed from the distorted version g. Therefore, image restoration concentrates on achieving an improved image $\hat{f}$, which is as close as possible to the original image.

Many restored images, which appear to be numerically good approximations to the original image, are, however, liable to incur the phenomenon of ringing (over- and undershoots, superblacks and whites). Since it is known that most original scenes are without ringing, such restoration results are usually undesirable. Two different classes of ringing effects have to be distinguished in restored images, namely,

i) ringing near the boundaries of the image, and

ii) ringing in the vicinity of steep intensity transitions (such as edges and bright point sources).

In [4], Woods *et al.* showed that the first type of ringing results from the intensity jumps at the boundaries of the blurred images, which introduce leakage frequencies. During the deconvolution action of the restoration filter, the leakage frequencies which are close to the zero crossings of the transfer function of the blurring system will be amplified, in this way introducing the ringing phenomenon. Several methods have been proposed which are capable of effectively reducing these kinds of ringing artifacts [4], [3].

The second class of ringing effects, which occur particularly strongly in linear space-invariant (LSI) restoration filters, is generally due to the poor match between the stationary assumed image model and the actual image data. In [5], Tekalp *et al.* describe a multiple image model restoration algorithm in which a number of image models is used to filter an image in agreement with the local edge orientations. Although good restorations were observed for synthetic images, the quality improvements obtained for images of real scenes were considerably less because real images cannot be adequately summarized using only a limited number of image models.

In this paper, we propose a flexible approach to the reduction of ringing near sharp intensity transitions. To this end, in Section II, we first analyze the origin of ringing in linear space-invariant image restoration filters, ending up with two possible methods to reduce these artifacts. Next, in Section III, a regularized iterative image restoration algorithm is proposed, in which the concepts of norms in a weighted Hilbert space and projections onto convex sets are used to include both ringing reduction methods. In Section IV, we demonstrate the significance

Manuscript received March 10, 1987; revised March 17, 1988.

The authors are with the Information Theory Group, Department of Electrical Engineering, Delft University of Technology, P.O. Box 5031, 2600 GA Delft, The Netherlands.

IEEE Log Number 8824225.

of our approach by several experimental results on noisy blurred images.

II. On the Origin of Ringing in Linear Space-Invariant (LSI) Image Restoration

In this section, we first discuss the concept of regularization. Two important representatives of regularized LSI image restoration filters, namely, the constrained least-squares filter and an iterative filter, are briefly reviewed. Next, a general expression is derived that characterizes ringing effects near sharp intensity transitions in images restored by any LSI filter. Finally, two methods will be discussed to reduce these ringing artifacts.

A. LSI Image Restoration Filters

In LSI image restoration, (1) reduces to the following two-dimensional discrete convolution:

$$g(i,j) = d(i,j) * f(i,j) + n(i,j), \tag{2}$$

where i, j are the spatial coordinates, and where $d(i,j)$ is the space-invariant point-spread function (PSF) of the blurring system. A direct solution to (2) can be obtained by using the convolutional inverse of $d(i,j)$. In the Fourier domain, the inverse filtered image is then given as

$$\hat{F}(u,v) = \frac{G(u,v)}{D(u,v)} = F(u,v) + \frac{N(u,v)}{D(u,v)}, \tag{3a}$$

where G, D, F, and N are the discrete Fourier transforms of g, d, f, and n, respectively, and where u, v are the spatial frequency variables [6]. The restoration error is given as

$$\left\|\hat{F}(u,v) - F(u,v)\right\| = \left\|\frac{N(u,v)}{D(u,v)}\right\| = \sqrt{\sum_{u,v}\left|\frac{N(u,v)}{D(u,v)}\right|^2}. \tag{3b}$$

It is, however, well known that the inverse problem (2) is ill posed or ill conditioned [7]–[10]. As a consequence, the restoration error will take very large values, particularly resulting from amplified high-frequency noise. Therefore, (3a) yields useless solutions in which the desired solution $F(u,v)$ is masked by amplified noise.

From the regularization theory [10], it is well known that physically meaningful solutions to ill-posed problems can be obtained by incorporating *a priori* information about the original data or the noise into the solution method. Since images usually have their major energy contributions in the low-frequency range, a smoothness condition is both physically realistic and acceptable *a priori* knowledge which may be used to regularize the ill-posed image restoration problem, in this way suppressing the amplification of noise in the high-frequency bands. If $L(u,v)$ represents the DFT of a general LSI regularizing operator, then the regularized restored image is obtained by minimizing [11]

$$\Omega(\hat{F}) = \left\|L(u,v)\hat{F}(u,v)\right\|, \tag{4}$$

subject to the condition that the norm of the noise is known:

$$\left\|G(u,v) - D(u,v)\hat{F}(u,v)\right\| = \left\|N(u,v)\right\|. \tag{5}$$

The above constrained minimization problem leads to the constrained least-squares or Tikhonov–Miller regularized solution [1], [10]–[12]:

$$\hat{F}(u,v) = \frac{D^*(u,v)}{\left|D(u,v)\right|^2 + \alpha\left|L(u,v)\right|^2} G(u,v), \tag{6}$$

where the regularization parameter α has to be chosen to validate (5). Other methods to select feasible values for α have been reported in the literature as well [11]–[14]. Various ways to define $L(u,v)$ are discussed in [1], [10], [11], and [27].

In several places in the literature, another regularization method of interest has been proposed. In this method, the (pseudo-)inverse filter is approximated iteratively, but the iterations are terminated prior to convergence when a certain (objective or subjective) criterion is satisfied [7], [15]–[17]. In the frequency domain, this iteration scheme is given by

$$\begin{aligned}\hat{F}_0(u,v) &= 0,\\ \hat{F}_{k+1}(u,v) &= \hat{F}_k(u,v) + \beta D^*(u,v)\\ &\quad\cdot\left(G(u,v) - D(u,v)\hat{F}_k(u,v)\right),\end{aligned} \tag{7}$$

where $\hat{F}_0(u,v)$ is the initial estimate, and where the relaxation parameter β controls the convergence of the iterations. An explicit expression for $\hat{F}_k(u,v)$ can easily be derived:

$$\begin{aligned}\hat{F}_k(u,v) &= \sum_{i=0}^{k-1}\left(1 - \beta\left|D(u,v)\right|^2\right)^i \beta D^*(u,v)G(u,v)\\ &= \frac{1 - \left(1 - \beta\left|D(u,v)\right|^2\right)^k}{D(u,v)} G(u,v).\end{aligned} \tag{8}$$

Equation (8) constitutes a linear space-invariant restoration filter with a regularization parameter proportional to $1/k$. For $1/k \to 0$, (7) converges to the nonregularized (pseudo-)inverse filter, provided that $|1 - \beta|D(u,v)|^2| < 1$.

B. Analysis of Ringing Effects

Consider a general linear space-invariant regularized restoration filter, which is characterized by its transfer function $H(u,v;\alpha)$. The regularization parameter α is the only free parameter in this transfer function, and α is in the range of 0 to ∞. Examples of $H(u,v;\alpha)$ can be derived from (6) or (8). Note that $\alpha \sim 1/k$ in (8).

The restored image $\hat{F}(u,v)$ is given by

$$\hat{F}(u,v) = H(u,v;\alpha)G(u,v). \tag{9}$$

Because of the regularization, $H(u, v; \alpha)$ deviates from the inverse of the blur, $D^{-1}(u, v)$. This deviation is expressed by the error spectrum $E(u, v; \alpha)$ [26]

$$E(u, v; \alpha) = 1 - H(u, v; \alpha)D(u, v). \quad (10)$$

By substituting $G(u, v)$, obtained from (2), into (9), and by using (10), we arrive at

$$\begin{aligned}\hat{F}(u, v) &= H(u, v; \alpha)\big(D(u, v)F(u, v) + N(u, v)\big) \\ &= F(u, v) - E(u, v; \alpha)F(u, v) \\ &\quad + \big(1 - E(u, v; \alpha)\big)D^{-1}(u, v)N(u, v),\end{aligned} \quad (11)$$

where $D^{-1}(u, v)$ should be replaced by the pseudoinverse $D^{\#}(u, v)$ if $D(u, v)$ has exact spectral zeros. From (11) we obtain

$$\begin{aligned}&\hat{F}(u, v) - F(u, v) \\ &\quad = -E(u, v; \alpha)F(u, v) \\ &\qquad + \big(1 - E(u, v; \alpha)\big)D^{-1}(u, v)N(u, v).\end{aligned} \quad (12)$$

Hence, the restoration error is given by

$$\begin{aligned}&\big\|\hat{F}(u, v) - F(u, v)\big\| \\ &\quad \le \big\|E(u, v; \alpha)F(u, v)\big\| \\ &\qquad + \big\|\big(1 - E(u, v; \alpha)\big)D^{-1}(u, v)N(u, v)\big\| \\ &\quad = E_1(\alpha) + E_2(\alpha).\end{aligned} \quad (13)$$

The corresponding expressions in the spatial domain are

$$\begin{aligned}&\hat{f}(i, j) - f(i, j) \\ &\quad = -e(i, j; \alpha) * f(i, j) \\ &\qquad + \big(1 - e(i, j; \alpha)\big) * d^{-1}(i, j) * n(i, j),\end{aligned} \quad (14)$$

and

$$\begin{aligned}&\big\|\hat{f}(i, j) - f(i, j)\big\| \\ &\quad \le \big\|e(i, j; \alpha) * f(i, j)\big\| \\ &\qquad + \big\|\big(1 - e(i, j; \alpha)\big) * d^{-1}(i, j) * n(i, j)\big\|,\end{aligned} \quad (15)$$

where the error sequence $e(i, j; \alpha)$ is defined as the inverse DFT of $E(u, v; \alpha)$. Clearly, the error in $\hat{f}(i, j)$ consists of two contributions. First, $E_1(\alpha)$ denotes the error due to the use of a regularized filter H instead of the inverse filter D^{-1}, i.e., the regularization error. Second, $E_2(\alpha)$ denotes the magnification of the random observation noise $n(i, j)$, i.e., the noise magnification error. This error is due to the ill posedness of the restoration problem. By studying the relations (12)–(15) and the properties of the two error contributions, we can gain greater understanding in the degradations in the restored image due to regularization.

General properties of $E_1(\alpha)$ and $E_2(\alpha)$, which follow directly from the concept of regularization, are [9], [10]

$$\lim_{\alpha \to 0} E_1(\alpha) = 0, \quad (16)$$

$$\lim_{\alpha \to 0} E_2(\alpha) \to \infty, \quad (17)$$

$$\lim_{\|n(i,j)\| \to 0} E_2(\alpha) = 0, \quad \text{for any } \alpha. \quad (18)$$

For given $\|n(i, j)\|$, the optimal solution $\hat{f}(i, j)$ is theoretically determined by the value of α which minimizes the total restoration error $E_1(\alpha) + E_2(\alpha)$. For the two types of errors implied by (6) and (8), there exists at least one optimal value of α since $E_1(\alpha)$ is a monotonically increasing function of α, and $E_2(\alpha)$ is a monotonically decreasing function. The optimal value of the regularization parameter is SNR dependent because the noise magnification error, $E_2(\alpha)$, is linearly proportional to $\|n(i, j)\|$.

The noise magnification error has a global degrading effect because it results from a globally random phenomenon—the observation noise. On the other hand, the regularization error is a function of f, and its effect will therefore be related strongly to the local structures encountered within the image. Ringing artifacts, a structure dependent phenomenon, should therefore be classified as a regularization error, i.e., are due to the fact that $H(u, v; \alpha)$ deviates from $D^{-1}(u, v)$. To make this relation more clear, we focus on the properties of the error spectrum and its related error sequence.

Unfortunately, general expressions defining the properties of $E(u, v; \alpha)$ and $e(i, j; \alpha)$ can hardly be derived since they depend on the specific restoration filter considered, the type of blur, and the severity of this blur. However, for a wide range of blurs and restoration filters of interest, at least one and often two of the following general characteristics will hold:

i) since $D(u, v)$ is generally some type of low-pass filter, $E(u, v; \alpha)$ has the shape of a high-pass filter; and

ii) $E(u, v; \alpha)$ has the shape of a bandpass filter near zero crossings of $D(u, v)$, with $E(u, v; \alpha) = 1$ for true spectral zeros. Since practical blurs of interest have multiple (equally spaced) zero crossings, $E(u, v; \alpha)$ takes the form of a multiple bandpass filter.

Both properties follow from the fact that balancing $E_2(\alpha)$ to $E_1(\alpha)$ requires $(1 - E(u, v; \alpha))$ to suppress the inverse filtered noise $D^{-1}(u, v)N(u, v)$ particularly in those spectral regions where $|D(u, v)| \to 0$. It is well known that filtering an image with a high-pass filter with characteristic frequency ω_c gives rise to ringing artifacts with a period of $2\pi/\omega_c$ samples (or Gibb's oscillations as they are usually called in this context). These artifacts, however, become far more pronounced when $E(u, v; \alpha)$ contains bandpass sections which are approximately equally spaced with distance ω_c (such as in motion blur). In conclusion, particularly the combination of the above-mentioned characteristics of $E(u, v; \alpha)$ will give rise to severe and widely distributed ringing artifacts in restored images.

In the sequel, we study the error spectrum and error sequence of the two types of LSI restoration filters described in the previous section. We select linear motion blur over N pixels along the horizontal axis as the image blur since this type of blur is known to represent a worst-case situation with respect to the severity and distribution of the ringing effects. In Fig. 1, a "cameraman" image (with size 256 × 256 pixels) is shown, which has been distorted by linear motion blur over $N = 8$ pixels and by additive noise with SNR = 30 dB. The restoration result using the constrained least-squares filter is given in Fig. 2 (with $L(u, v)$ = Laplace filter, $\alpha = 0.001$), in which the ringing is clearly present. In Fig. 3(a), the modulus of the sinc-shaped transfer function of the blur has been plotted. By combining (6) and (10), the error spectrum for the constrained least-squares filter is obtained [26]:

$$E(u, v; \alpha) = \left[1 + \frac{|D(u, v)|^2}{\alpha |L(u, v)|^2} \right]^{-1}. \qquad (19)$$

The error spectrum for various values of the regularization parameter α has been plotted in Fig. 3(b), while the error sequences are shown in Fig. 3(c). Observe that particularly when the error spectrum tends to have peaks (at $\pm 2\pi/N$), the error sequence is dominated by positive impulses at $i = \pm kN$ [Fig. 3(d)].

In the spatial domain, the regularization error is a convolution of $-e(i, j; \alpha)$ with $f(i, j)$. In flat regions of the image, this convolutional action has hardly any effect, but in the vicinity of steep intensity transitions, it will cause negative versions of the intensity transitions to appear at distances $\pm kN$ ($k = 1, 2, \cdots$). The severity of the ringing artifacts [determined by the distribution and the size of the positive spikes in $e(i, j; \alpha)$] depends on the value of α. Since the optimal value of α, which minimizes the restoration error, is SNR dependent, the severity of ringing artifacts is a function of the SNR as well. An interesting detail of this relation is that the ringing is negligible for both very small values of α (high SNR) as well as for large values of α (low SNR), although $E_1(\alpha)$ itself is monotonically increasing function of α. Clearly, for low SNR's, the restoration filter has degenerated to a low-pass noise smoothing filter, in which the regularization error manifests itself no longer as ringing, but as severe blurring of edges. It should be kept in mind that Fig. 3 refers to just one type of distortion, and that the behavior of the error spectrum and error sequence are strongly related to the type and severity of the distortion.

The error spectrum for the iterative restoration filter formulated in (7) is easily found to be [18], [26]

$$E\left(u, v; \frac{1}{k}\right) = \left(1 - \beta |D(u, v)|^2\right)^k. \qquad (20)$$

The error spectrum and the error sequence for different values of the iteration index k are shown in Fig. 4. Observe that particularly for a small number of iterations

Fig. 1. Cameraman image blurred by horizontal linear motion over 8 pixels and noise added with SNR = 30 dB.

Fig. 2. Constrained least-squares restoration from Fig. 1 showing severe ringing artifacts.

(corresponding to a large value of the related regularization parameter), the ringing effects will be relatively severe.

Since both the constrained least-squares filter (6) and the iterative scheme (7) have the pseudoinverse filter as their "limiting filter" (for $\alpha \to 0$ and $k \to \infty$, respectively), we finally consider the error spectrum of this filter. The limiting spectrum of both (19) and (20) is

$$E(u, v) = \begin{cases} 1, & \text{if } |D(u, v)| = 0, \\ 0, & \text{if } |D(u, v)| \neq 0. \end{cases} \qquad (21)$$

Fig. 5 shows the error spectrum and the error sequence (with an enlarged vertical axis) of this nonregularized filter, which introduces hardly any ringing, but cannot prevent noise magnification either.

C. Two Methods to Reduce Ringing

The analysis in the previous section has shown that in regularizing the image restoration problem, we have to deal with two counterproductive phenomena: the noise magnification error and the regularization error. Ringing effects near sharp intensity transitions in the restored images are attributable to the regularization. Since in LSI restoration filters the behavior of the two types of errors is controlled by (13) and (15), the appearance of excessively amplified noise, ringing effects, or a combination of these two is inevitable. We therefore have to consider restoration methods which are not based on LSI filters.

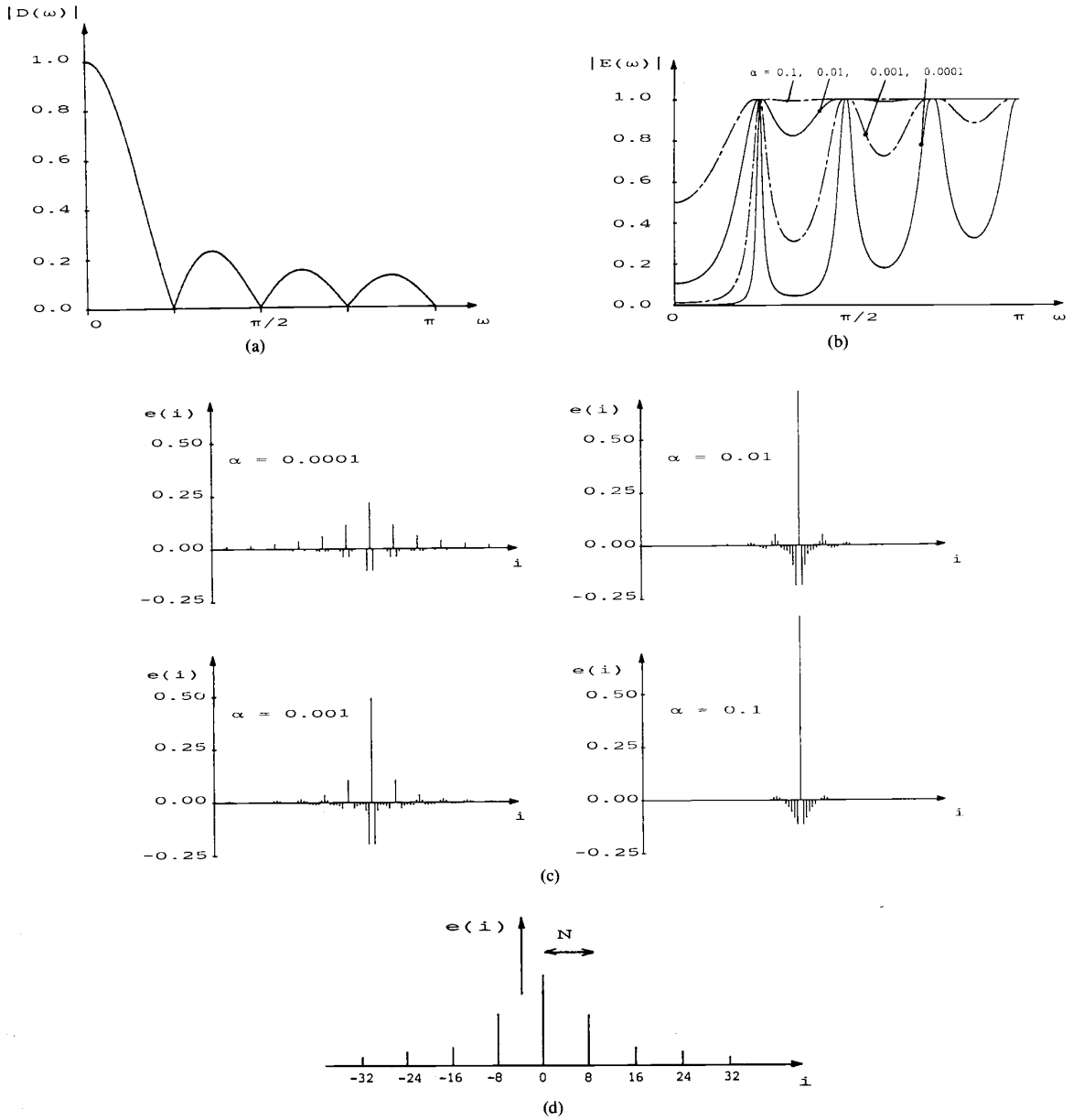

Fig. 3. Properties of the regularization error of the constrained least-squares filter for linear motion blur over 8 pixels. (a) Modulus of the transfer function, (b) modulus of the error spectrum, (c) error sequence, (d) typical behavior of the dominant impulses in an error sequence.

Deterministic A Priori Knowledge About the Original Image: In image restoration, it is usually *a priori* known that most original scenes are without ringing. Therefore, the restoration results can be improved by using this deterministic knowledge in the restoration process in the form of constraints on the solution. If the image data, for example, consist of blurred bright point sources against a black background (such as occurs in astronomical imaging), then the ringing will be visible as negative intensity values. The knowledge about the positivity of the original data may then be used to replace all negative values by zero, thus eliminating the ringing completely.

The relatively simple class of LSI restoration filters cannot utilize these kinds of constraints, which are often nonlinear and space-variant. In recent years, fruitful use has been made of the theory of the projections onto convex sets [36] in developing iterative restoration algorithms which incorporate many kinds of *a priori* constraints [19]–[23]. The work by Trussell and Civanlar [20], [33], Sezan *et al.* [21], [23], and others in the field

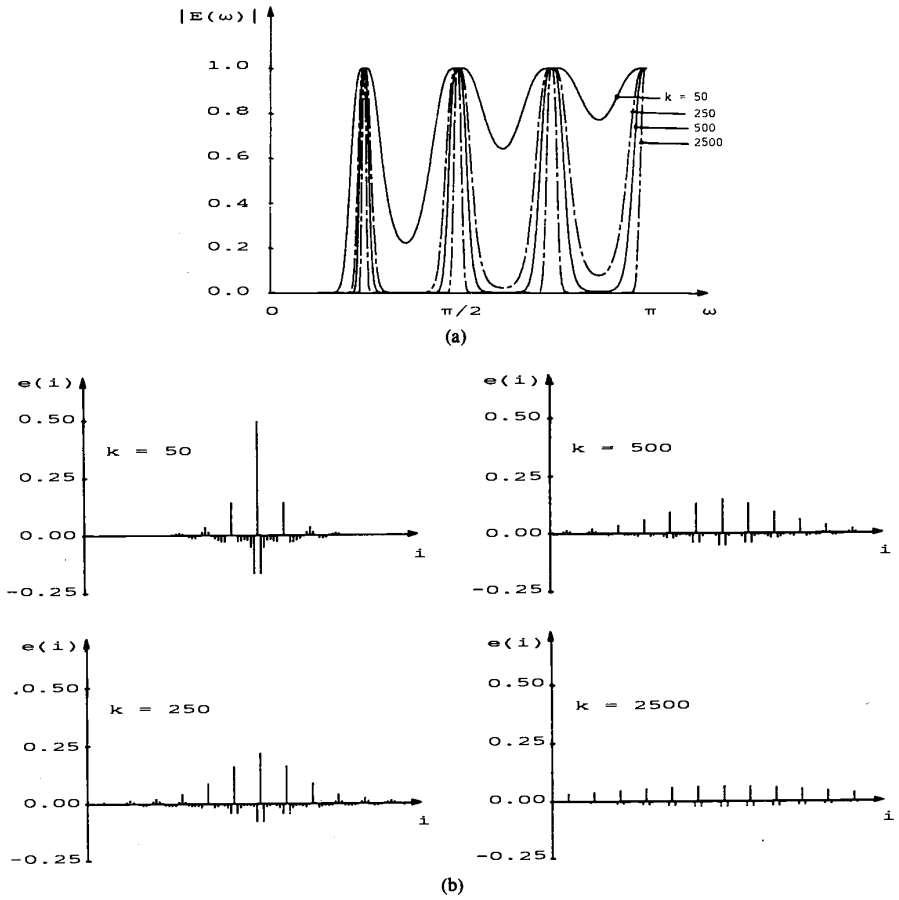

Fig. 4. Properties of the regularization error of the iterative scheme (7) for linear motion blur over 8 pixels. (a) Modulus of the error spectrum, (b) error sequence.

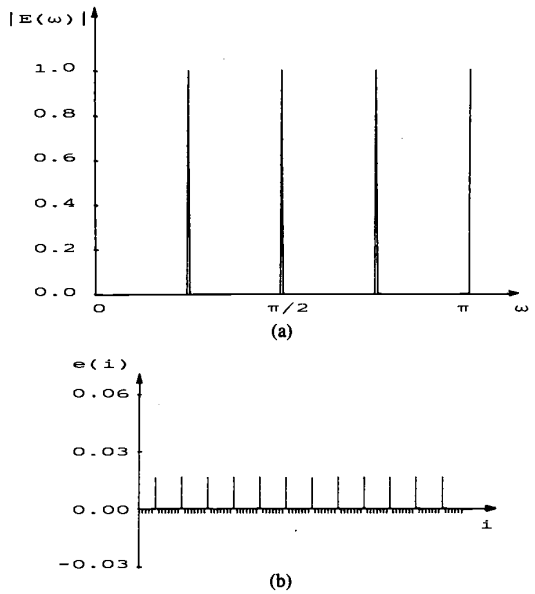

Fig. 5. Properties of the regularization error of the pseudoinverse filter for linear motion blur over 8 pixels. (a) Modulus of the error spectrum, (b) error sequence (note the enlargement of the vertical scale).

of restoration using the method of the convex projections has shown that this technique yields good results when the *a priori* knowledge describes the original image accurately enough.

Another method to incorporate deterministic constraints in restoration procedures is the constrained minimization technique. The power of this method has been experienced by many researchers in the field of band-limited extrapolation, reconstruction from phase, and constrained deconvolution [15]. Again, these methods work very well when the constraints describe the original image accurately enough. Unfortunately, such powerful constraints can usually not be obtained when dealing with the restoration of more complicated signals, such as images of natural scenes. In these situations, the use of deterministic constraints is usually insufficient to significantly reduce the ringing artifacts.

Adaptivity of the Restoration Algorithm: Ringing artifacts are caused by the global minimization of (13) and (15) with respect to α. Obviously, a smaller restoration error can be achieved by adapting this minimization process to the local image properties. The adaptive (space-variant) version of (14) becomes

$$\hat{f}(i,j) - f(i,j) = -e(i,j;k,\ell;\alpha) * f(i,j) + \big(1 - e(i,j;k,\ell;\alpha)\big) * d^{-1}(i,j) * n(i,j), \quad (22)$$

with the space-variant PSF of the restoration filter given by

$$h(i,j;k,\ell;\alpha) = \big(1 - e(i,j;k,\ell;\alpha)\big) * d^{-1}(i,j). \quad (23)$$

Adaptive restoration now focuses on designing $e(i,j;k,\ell;\alpha)$ in such a way that the restoration error resulting from (22) is smaller than the one in (15), through which the regularization error is reduced as well. Furthermore, the complexity of the space-variant filter $h(i,j;k,\ell;\alpha)$ should be acceptable from a computational point of view.

As an example, we consider the required behavior of $e(i,j;k,\ell;\alpha)$ in the vicinity of two extreme local properties encountered in images, namely, edge regions and relatively smooth areas. Near sharp intensity transitions, the regularization error dominates the noise magnification error, while in the more gradual areas the convolution of $f(i,j)$ with $-e(i,j;k,\ell;\alpha)$ has hardly any effect, so that $E_2(\alpha)$ dominates $E_1(\alpha)$. Consequently, $e(i,j;k,\ell;\alpha)$ should be adapted in such a way that the regularization error becomes smaller in edge regions. As a result, the ringing artifacts will be reduced, but more noise will be introduced since the regularization error and the noise magnification error are counterproductive. In the more gradual image regions, the opposite regulation of $e(i,j;k,\ell;\alpha)$ should be accomplished in order to reduce the noise magnification error, while keeping the regularization error at a nearly constant level.

Besides the above arguments, adaptive restoration is also supported by properties of the human visual system. Although the characteristics and responses of the human visual system are very complex, we know from various psychophysical experiments that the visibility of noise is greatly masked by sharp intensity transitions, whereas blurring generally appears to be unacceptable in this context [24], [27]. This noise masking effect validates decreasing the regularization error and increasing the noise magnification error near edges in order to prevent ringing from happening. In relatively flat regions, the restoration process has to emphasize the noise smoothing because blurring will barely visible in these regions, but noise will give rise to extraordinary features to the observer.

In conclusion, by using an adaptive regularization method, the appearance of ringing effects can be reduced, smaller restoration errors can be achieved, and visually better results are arrived at.

III. Iterative Image Restoration in a Weighted Hilbert Space

In this section we propose a novel regularized iterative image restoration algorithm. Deterministic *a priori* knowledge about the original image is incorporated into the algorithm by applying a projection operator in every iteration step. The concept of norms in a weighted Hilbert space is used to adapt the restoration process to local properties in the image [25], [26]. By the use of weighting matrices, we implicitly define locally varying error sequences $e(i,j;k,\ell;\alpha)$.

The matrix-vector notation introduced in (1) will be used throughout this section to allow (if necessary) a space-variant blur description.

A. A Priori Knowledge

In image restoration, we usually have available an estimate of the norm of the noise present in the blurred image. A set of feasible solutions can then be defined by restricting the norm of the residual $g - D\hat{f}$ to this noise norm [20], [27], [28]. Such a global norm would result in an equal distribution of the noise magnification error and the regularization error throughout the restored image. The local regulation of the two types of errors can be achieved by defining the norm of the residual in a weighted space:

$$\|g - D\hat{f}\|_R = \left[(g - D\hat{f})^t R (g - D\hat{f})\right]^{1/2} \le \epsilon. \quad (24)$$

Here R is a diagonal matrix containing weight coefficients $r_{ij} \in [0, 1]$ for the picture element (i,j). The bound ϵ is assumed *a priori* known, and is related to the amount of noise present in the blurred image. The computation of the values for r_{ij} will be discussed later in this section.

The (Tikhonov–Miller) regularization, as described in Section II-A, provides the second kind of *a priori* knowledge. To regulate locally the tradeoff between the noise magnification error and the regularization error, we propose imposing an upper bound on the norm of the filtered image $L\hat{f}$ in a weighted space, where L is the linear regularizing operator

$$\|L\hat{f}\|_S = \left[(L\hat{f})^t S (L\hat{f})\right]^{1/2} \le E. \quad (25)$$

Here S is again a diagonal weighting matrix containing positive coefficients $s_{ij} \in [0, 1]$. The bound E is assumed to be (approximately) known *a priori*.

Finally, the third kind of *a priori* knowledge is a (combination of) deterministic constraint(s). The set of solutions C described by this constraint has to be convex and closed [19], [22]. We can then define the orthogonal nonexpansive projection P onto this convex set as

$$P\hat{f} = \begin{cases} \hat{f}, & \text{if } \hat{f} \in C, \\ h, & \text{if } \hat{f} \notin C, \end{cases} \quad (26)$$

where $h \in C$, and $\|h - \hat{f}\| \le \|x - \hat{f}\|, \quad \forall x \in C.$

The solution to the restoration problem is required to be an element of the set C, hence, it has to be a fixed point of the projection P.

The weight coefficients r_{ij} and s_{ij} in (24) and (25), respectively, have to be chosen on the basis of prior knowl-

edge about the original image in order to minimize the restoration error. Clearly, such information is hardly ever available, which makes the computation of the optimal weight coefficients impossible for practical situations of interest. For this reason we have to adopt a more practical point of view. For example, we can base these coefficients on a local variance measure computed from the blurred image itself [25], [27], [29], or compute them from a preliminary nonadaptive restoration result [25]. Qualitatively, we observe that in order to reduce ringing artifacts by decreasing the regularization, near sharp intensity transitions, we have $s_{ij} \ll 1$ and $r_{ij} \cong 1$ (enforcing pseudoinverse filtering). On the other hand, to smooth the noise in the more gradual regions, we have $s_{ij} \cong 1$ and $r_{ij} \ll 1$.

It is worthwhile noticing that the weighting matrix R may also account for the nonstationarity of the noise variance. If the noise has a local variance $\sigma_n^2(i, j)$ in the picture element (i, j), the weight coefficients r_{ij} are assigned the reciprocal value of $\sigma_n^2(i, j)$, or

$$R = \Phi_n^{-1}. \tag{27}$$

where Φ_n is the (diagonal) autocorrelation matrix of the noise. In a worst case situation, some image elements may have been corrupted in such a serious way (for example, due to data transmission or recording errors) that their erroneous values must be excluded from the restoration process. This is achieved by assigning the value zero to the corresponding weight coefficients r_{ij}.

B. Formulation of the Algorithm

Following the Miller regularization approach [12], we combine (24) and (25) into a single quadrature formula

$$\Phi(\hat{f}) = \| g - D\hat{f} \|_R^2 + \alpha \| L\hat{f} \|_S^2 \leq 2\epsilon^2. \tag{28}$$

The regularization parameter has the fixed value $\alpha = (\epsilon/E)^2$. If a solution $\hat{f}$ satisfies the bounds in (24) and (25), then it will also satisfy (28). Conversely, if a solution $\hat{f}$ satisfies (28), then (24) and (25) are also satisfied except for a factor of at most $\sqrt{2}$ [12], which is insignificant for practical cases.

Among the solutions satisfying (28), a physically reasonable choice is the solution $\hat{f}_m$, called the Miller regularized solution, which minimizes the functional $\Phi(\hat{f})$. The solution of this minimization problem is given by the normal equations

$$(D^tRD + \alpha L^tSL)\hat{f}_m = D^tRg. \tag{29}$$

If there exists at least one solution which satisfies (28), then $\hat{f}_m$ will satisfy (28) as well.

In this paper we require $(D^tRD + \alpha L^tSL)$ to be a nonsingular matrix yielding a unique Miller solution. This is not a severe restriction since exact spectral zeros occur rarely in practical situations of interest. The extension to singular matrices is straightforward by considering generalized inverses instead of true inverse matrices.

Observe that if we assume the images of size $M \times N$, the direct computation of $\hat{f}_m$ would require the matrix $(D^tRD + \alpha L^tSL)$ of size $MN \times MN$ to be inverted. Because this matrix represents a space-variant operator, we cannot reduce the computational complexity by applying the standard diagonalization procedure for block-circulant matrices, i.e., Fourier domain filtering [6]. Furthermore, we cannot guarantee that the solution $\hat{f}_m$ will satisfy the constraint C, nor can (29) be modified so that the deterministic condition is always met. For these reasons, the solution $\hat{f}_m$ is approximated by using an iterative method, which simultaneously offers the possibility of imposing a deterministic constraint on the solution.

Following [15], we rewrite (29) as

$$\begin{aligned}\hat{f}_m &= (I - \alpha\beta L^tSL)\hat{f}_m + \beta D^tR(g - D\hat{f}_m) \\ &= G(\hat{f}_m),\end{aligned} \tag{30}$$

where β is the contraction or relaxation parameter. The unique fixed point of the mapping G coincides with the solution of (29), and can be computed by the contraction mapping theorem [22], yielding the following iterative scheme:

$$\hat{f}_{k+1} = G(\hat{f}_k). \tag{31}$$

Here k is the iteration index ($k = 0, 1, 2, \cdots$). A sufficient condition for the convergence of these iterations is the contractiveness of the mapping G. This requirement leads to the following bounds for the relaxation parameter (Appendix A):

$$0 < \beta < \frac{2}{\lambda_{\max}}, \tag{32}$$

where $\lambda_{\max}$ is the largest eigenvalue of the matrix $(D^tRD + \alpha L^tSL)$.

The deterministic constraint C is introduced in the algorithm by applying the projection operator P in every iteration step:

$$\hat{f}_{k+1} = P\,G(\hat{f}_k). \tag{33}$$

The iterations in (33) converge to the unique fixed point $\hat{f}_l$ of the concatenated mapping $P\,G$ in the convex set C, provided that $P\,G$ is a contraction mapping. Since the projection operator P is nonexpansive by definition, $P\,G$ will be contractive if G is a contraction mapping [19], [21], [22]. Hence, sufficient converge conditions for the iterations in (33) are given by the bounds on β in (32).

Although theoretically no restrictions are imposed on the initial estimate $\hat{f}_0$, it is sensible to select an initial estimate which already shows some of the desired properties, possibly combined with an appropriate constraint C [23]. A common choice is $\hat{f}_0 = g$, but more sophisticated initial estimates may improve the restoration result and the convergence behavior of the algorithm [20], [23], [31]. Substituting the definition of the mapping G into (33) yields the regularized iterative image restoration in a

weighted Hilbert space:

$$\hat{f}_0 = g,$$

$$\hat{f}_{k+1} = P[(I - \alpha\beta L^t SL)\hat{f}_k + \beta D^t R(g - D\hat{f}_k)]. \quad (34)$$

We note that the proposed algorithm is in fact a constrained steepest descent algorithm [32]. In Appendix B, we show that the limiting solution $\hat{f}_l$ of the iterative algorithm in (34) minimizes the functional $\Phi(\hat{f})$ subject to the deterministic constraint C. Hence, if there exists a solution which satisfies both (28) and the constraint C, it will be obtained by the iterative scheme in (34). Furthermore, within the set of solutions satisfying both (28) and the constraint C, the iterations in (34) converge to the solution $\hat{f}_l$ which minimizes $\Phi(\hat{f})$. It is, therefore, guaranteed that the Miller solution $\hat{f}_m$ is optimally approximated within the set C. Clearly, $\hat{f}_l$ will coincide with the Miller solution if the latter is an element of the set C (consistency of the iterative scheme). The substitution of the limiting solution $\hat{f}_l$ in (28) gives an *a posteriori* check on the claimed noise norm, the bound E, and the *a priori* knowledge represented by the convex set C for the given blurred image g.

In recent years, various iterative algorithms have been proposed comparable to the one in (34) [7], [15], [16], [25]–[30], [32]. Katsaggelos *et al.* [27]–[30] were the first to apply the Miller regularization together with an iterative solution technique to the image restoration problem. They also proposed various adaptive iterative schemes, such as in [27] and [29] where the term $(I - \alpha\beta L^t SL)$ in (34) appears as one single adaptive noise smoothing filter (e.g., of the Wiener type). In [30], adaptivity was introduced by spatially varying the value of the regularization parameter α. Such an approach is strongly related to using a weighting matrix S.

We observe that the stabilizing term $(I - \alpha\beta L^t SL)\hat{f}_k$ is generally a low-pass filtering action which partially removes the high frequencies from the iterations. Depending on the values of the weight coefficients in the S matrix, the low-pass filtering is very active (large coefficients) or nearly disabled (small coefficients).

The adaptivity introduced by the weighting matrix R in (24) locally regulates the size of the restoration term $\beta D^t R(g - D\hat{f}_k)$. This may also be interpreted as locally varying the relaxation parameter β, which has been suggested as well by Ichioka *et al.* on more practical grounds [16]. In this sense, (34) can be considered a general formulation of this class of constrained minimization algorithms.

IV. Experimental Results

The performance of the proposed iterative image restoration filter in (34) is illustrated by three examples on artificially blurred images in this section. The results will be compared to the restoration results of the constrained least-squares filter because this is a typically regularized, linear space-invariant restoration filter. Since we simulated the blurring of the images, we have available the perfect boundary conditions to suppress the ringing artifacts near the boundaries. In the experiments, we concentrate on reducing ringing effects which are caused by regularizing the image restoration problem.

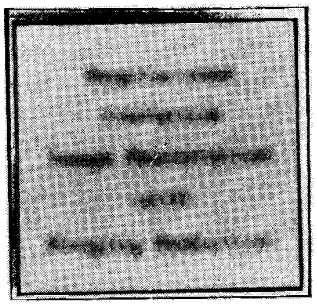

Fig. 6. Defocused text image and noise added with SNR = 30 dB.

The filter performance is measured with the well-known improvement in SNR:

$$\text{SNR improvement} = 10 \log_{10} \frac{\|f - g\|^2}{\|f - \hat{f}\|^2}. \quad (35)$$

In all experiments, the $2-D$ Laplace filter was used as the regularizing operator L [11]. In order to obtain the true limiting solution $\hat{f}_l$, the iterations were continued until the changes in the restoration result were smaller than the machine accuracy ($\approx 10^{-6}$). It was observed that this is an extremely pessimistic convergence criterion, since the major improvements were gained in the first 5–10 percent of the iterations [32]. Alternative, less pessimistic convergence criteria may result in restored images with comparable performance [17].

Experiment 1: A "text image" of size 256 × 256 pixels with each pixel quantized in 8 bit was defocused by using the following pill-box model with a squared radius of 50 pixels for the PSF:

$$d(i,j) = \begin{cases} \dfrac{1}{161}, & \text{if } i^2 + j^2 \le 50, \\ 0, & \text{elsewhere.} \end{cases} \quad (36)$$

White Gaussian noise was added with SNR = 20, 30, 40, 50, and 60 dB, respectively. In Fig. 6, the blurred text image with SNR = 30 dB is shown. The restoration obtained by the constrained least-squares filter (6) is given in Fig. 7 ($\alpha = 5.10^{-5}$).

Although the numerical improvement of 5.5 dB is acceptable, the restored image shows disturbing ringing effects. Next, the regularized iterative restoration algorithm in (34) was used with the following projection operator to constrain the image intensities:

$$P[f(i,j)] = \text{Min}\{210, \text{Max}[f(i,j), 25]\}. \quad (37)$$

Since this projection operator represents very accurate knowledge about the original image intensities, the oc-

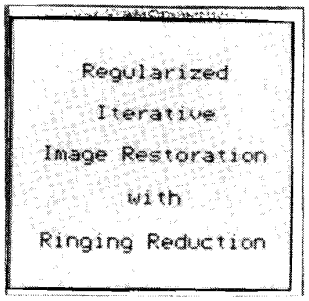

Fig. 7. Constrained least-squares restoration from Fig. 6 (SNR improvement = 5.5 dB).

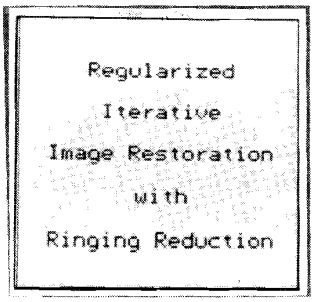

Fig. 8. Restoration by the regularized iterative restoration algorithm with an intensity constraint (SNR improvement = 10.8 dB).

TABLE I
SNR IMPROVEMENT FOR THE TEXT IMAGE DEFOCUSED BY THE PSF GIVEN IN (36), AND WITH WHITE GAUSSIAN NOISE ADDED OF VARIOUS SIGNAL-TO-NOISE RATIOS

	SNR IMPROVEMENT (dB)	
Signal-to-noise ratio (dB)	Constrained least-squares filter	Regularized iterative filter with projection operator
20	2.7	4.8
30	5.5	10.8
40	9.8	21.8
50	14.5	35.2
60	19.5	44.2

currence of ringing effects can be prevented completely. The restoration result, which has an SNR improvement of 10.8 dB, is shown in Fig. 8 (S = R = Identity, $\alpha = 5.10^{-5}$). In Table I, the SNR improvements for the various signal-to-noise ratios are listed for the constrained least-squares filter and the constrained regularized iterative restoration algorithm.

Experiment 2: The "cameraman image" in Fig. 9 (256 × 256 pixels, quantized in 8 bit) was defocused by using the following PSF:

Fig. 9. Original cameraman image.

Fig. 10. Defocused cameraman image, noise added with SNR = 30 dB.

$$d(i,j) = \frac{1}{20.0296}\begin{bmatrix} 0.1716 & 0.7929 & 1.0000 & 0.7929 & 0.1716 \\ 0.7929 & 1.0000 & 1.0000 & 1.0000 & 0.7929 \\ 1.0000 & 1.0000 & 1.0000 & 1.0000 & 1.0000 \\ 0.7929 & 1.0000 & 1.0000 & 1.0000 & 0.7929 \\ 0.1716 & 0.7929 & 1.0000 & 0.7929 & 0.1716 \end{bmatrix} \quad (38)$$

Noise was added to the blurred image with SNR = 20, 30, 40, 50, and 60 dB, respectively. Fig. 10 shows the blurred image with additive noise of 30 dB. The constrained least-squares restoration result with α chosen according to the Miller regularization ($\alpha = 0.001$) is shown in Fig. 11 (SNR improvement = 3.7 dB). To regulate locally the regularization, the blurred image was restored by the adaptive algorithm (34) using the weighting matrix S. First, the local variance $\sigma_g^2(i,j)$ was computed from the blurred image g [29]:

$$\sigma_g^2(i,j) = \frac{1}{(2P+1)(2Q+1)} \sum_{k=i-P}^{i+P} \sum_{l=j-Q}^{j+Q} \left[g(k,l) - m_g(i,j) \right]^2, \quad (39)$$

Fig. 11. Constrained least-squares restoration from Fig. 10 (SNR improvement = 3.7 dB).

Fig. 12. Restoration by the adaptive regularized iterative restoration algorithm with an intensity constraint (SNR improvement = 6.4 dB).

where $(2P + 1)(2Q + 1)$ is the size of the analysis window in which the local variance is computed, and where $m_g(i, j)$ is the local mean, given by

$$m_g(i, j) = \frac{1}{(2P + 1)(2Q + 1)} \sum_{k=i-P}^{i+P} \sum_{l=j-Q}^{j+Q} g(k, l). \tag{40}$$

In regions with slow intensity transitions, the local variance takes approximately the value of the noise variance, whereas the larger local variances correspond to the "edgy" regions in the image. Using this local variance measure, the coefficients in the weighting matrix S are computed as

$$s_{ij} = \frac{1}{1 + \mu \operatorname{Max}\left[0, \sigma_g^2(i, j) - \sigma_n^2\right]}, \tag{41}$$

where the noise variance σ_n^2 was estimated from a smooth image region, and where μ is a tuning parameter.

The restoration result obtained by (34) (with $\mu = 0.5$, $Q = P = 2$, and $\alpha = 0.05$), and with a projection operator constraining the image intensities to the interval [240, 10], is shown in Fig. 12. The SNR improvement for this restoration result is 6.4 dB. Table II lists the performance of the algorithm over a wider SNR range. Observe that the application of an intensity constraint is less effective than in Experiment 1, and does not give any additional improvement when the blurred image has a relatively high signal-to-noise ratio.

Experiment 3: The last experiment deals with the worst-case situation (with respect to ringing effects) of linear motion blur. The cameraman image was blurred by horizontal motion over 9 pixels and noise was added with SNR = 30 dB (Fig. 13). The constrained least-squares restoration result is shown in Fig. 14 ($\alpha = 0.001$), and has an SNR improvement of 5.5 dB. The restoration result obtained by the adaptive algorithm using the weighting matrix S, and using a projection operator to constrain the intensities to the range [240, 10], is shown in Fig. 15 ($\alpha = 0.05$, $\mu = 0.5$, $P = Q = 2$). The SNR improvement is 7.4 dB. Particularly in this worst-case situation, the restoration result has considerably less ringing artifacts. Table III lists the performances of the compared algorithms for various signal-to-noise ratios.

To simulate the severe corruption of image data due to a locally very large noise variance or recording errors, 50 percent of the pixels in the blurred image in Fig. 13 was randomly discarded (Fig. 16). The corresponding coefficients in the weighting matrix R were set to zero to exclude the erroneous data from the restoration process. The restoration result from this noisy blurred image with incomplete data is shown in Fig. 17, showing the combined effect of the two weighting matrices.

V. Conclusions and Discussion

Ringing effects near sharp intensity transitions in restored images are caused by the necessary regularization of the ill-posed image restoration problem. The use of deterministic *a priori* knowledge and the local adaptation of the noise magnification error and the regularization error (adaptive regularization) have been shown to be powerful means to prevent ringing artifacts from happening. Both ringing reduction methods have been fundamentally incorporated in an iterative restoration algorithm. The restoration results obtained by the proposed method show a favorable behavior in both numerical and visual respects.

A disadvantage of iterative restoration methods is the considerable computation it takes to obtain a (visually) stable solution due to the low convergence speed of this type of algorithm. Algorithms with an increased convergence speed, which are, for example, based on a conjugate gradients minimization method, have been recently developed, and have shown to offer an attractive alternative to the iteration (34) [32].

In some cases, (1) does not describe the image formation and recording process accurately enough due to a nonlinear response of the image sensor. In such situations, this model has to be extended with a sensor nonlinearity [1]. In [34] it is shown that the iterative algorithm proposed in this paper can easily be extended to account for such a sensor nonlinearity.

The two components of the functional to be minimized [(24), (25)] are, in fact, two convex sets. Conceptually it is therefore possible to compute a solution satisfying (24)–(26) using the method of the projections onto convex sets (P.O.C.S.), or techniques using fuzzy sets [33]. Such iterative algorithms are very likely to converge to solutions highly resembling the ones obtained by the iteration

TABLE II
SNR IMPROVEMENT FOR THE CAMERAMAN IMAGE DEFOCUSED BY THE PSF GIVEN IN (38), AND WITH WHITE GAUSSIAN NOISE ADDED OF VARIOUS SIGNAL-TO-NOISE RATIOS

Signal-to-noise ratio (dB)	SNR IMPROVEMENT (dB)		
	Constrained least-squares filter	Regularized iterative filter using the weighting matrix S	Regularized iterative filter using both the weighting matrix S and a projection
20	1.7	2.9	3.3
30	3.7	5.9	6.4
40	7.3	9.7	10.1
50	11.6	13.8	--
60	16.1	17.9	--

Fig. 13. Cameraman image blurred by horizontal linear motion over 9 pixels and noise added with SNR = 30 dB.

Fig. 14. Constrained least-squares restoration from Fig. 13 (SNR improvement = 5.5 dB).

Fig. 15. Restoration by the adaptive algorithm with an intensity constraint (SNR improvement = 7.4 dB).

(34) as long as the intersection of the convex sets is relatively small. Such an approach has the obvious advantage that more convex sets can be used. Unfortunately, the practical implementation of the projections onto the weighted sets (24) and (25) is computationally very demanding. For this reason, we have confined ourselves to the constrained iterative minimization method as presented in Section III.

Finally, we observe that the proposed algorithm, as is the case with many adaptive methods, requires a number of tuning parameters to be measured or estimated from the blurred data. The restoration results are relatively insensitive to the choice of these parameters. Therefore, of special interest to us, and the subject of our current investigation, is the study of automatic identification procedures for the tuning parameters, regularizing operator, and the unknown blurs [35].

APPENDIX A
CONTRACTIVENESS OF THE MAPPING G

The mapping G has been defined in (30) by

$$G(f) = (I - \alpha\beta L^t SL)f + \beta D^t R(g - Df)$$
$$= (I - \beta(D^t RD + \alpha L^t SL))f + \beta D^t Rg. \quad \text{(A1)}$$

This mapping is said to be contractive if the following condition holds:

$$\|G(f_1) - G(f_2)\| \leq \theta \|f_1 - f_2\|,$$
$$\text{with } f_1 \neq f_2, \quad \text{and } 0 < \theta < 1, \quad \text{(A2)}$$

where $\|\cdot\|$ is the regular Euclidean norm. When substituting (A1) into (A2), we arrive at

$$\|\{I - \beta(D^t RD + \alpha L^t SL)\}f_1$$
$$- \{I - \beta(D^t RD + \alpha L^t SL)\}f_2\|$$
$$\leq \|I - \beta(D^t RD + \alpha L^t SL)\| \cdot \|f_1 - f_2\|$$
$$\leq \theta \|f_1 - f_2\|, \quad \text{(A3)}$$

TABLE III
SNR IMPROVEMENT FOR THE CAMERAMAN IMAGE BLURRED BY HORIZONTAL LINEAR MOTION OVER 9 PIXELS, AND WITH WHITE GAUSSIAN NOISE ADDED OF VARIOUS SIGNAL-TO-NOISE RATIOS

Signal-to-noise ratio (dB)	SNR IMPROVEMENT (dB)		
	Constrained least-squares filter	Regularized iterative filter using the weighting matrix S	Regularized iterative filter using both the weighting matrix S and a projection
20	2.8	3.9	4.3
30	5.5	7.1	7.4
40	9.8	11.6	11.8
50	14.6	16.8	--
60	19.8	21.3	--

Fig. 16. 50 percent of the data in Fig. 13 discarded.

Fig. 17. Restoration of Fig. 16 by the adaptive algorithm.

which yields the following inequalities:

$$0 < \left\| I - \beta(D^tRD + \alpha L^tSL) \right\| < 1. \qquad \text{(A4)}$$

Since $(D^tRD + \alpha L^tSL)$ is a symmetrical matrix, both the eigenvalues of this matrix, denoted by λ_i, and the eigenvalues of $I - \beta(D^tRD + \alpha L^tSL)$ are real values. We can therefore replace (A4) by

$$0 < \operatorname*{Max}_i \left\{ \left| 1 - \beta\lambda_i \right| \right\} < 1, \qquad \forall i. \qquad \text{(A5)}$$

The bounds in (A5) are always satisfied if β satisfies the relation

$$0 < \beta < \frac{2}{\lambda_{\max}}, \qquad \text{(A6)}$$

where $\lambda_{\max}$ is the largest eigenvalue of the matrix $(D^tRD + \alpha L^tSL)$.

APPENDIX B
PROPERTIES OF THE LIMITING SOLUTION

In this appendix we prove that the algorithm in (34) minimizes the function $\Phi(f)$ [(28)] on the closed convex set C. First, we define the gradient of $\Phi(f)$ with respect to f

$$\psi(f) = -\tfrac{1}{2}\nabla_f\Phi(f), \qquad \text{(B1)}$$

where the constant $-\frac{1}{2}$ is introduced for notational simplicity. According to (30), the mapping $G(f)$ is created as

$$G(f) = f + \beta\psi(f). \qquad \text{(B2)}$$

The iterative algorithm is then given by

$$\hat{f}_{k+1} = P\,G(\hat{f}_k) = P\left[\hat{f}_k + \beta\psi(\hat{f}_k)\right]. \qquad \text{(B3)}$$

Since the mapping G is required to be contractive, and the mapping P is nonexpansive, the concatenated mapping $P\,G$ is a contraction mapping. By the contraction mapping theorem, the iterations in (B3) converge to the unique fixed point $\hat{f}_l$ of the mapping $P\,G$. As a consequence, the following relation has to hold for $\hat{f} = \hat{f}_l$:

$$\hat{f}_l = P\left[\hat{f}_l + \beta\psi(\hat{f}_l)\right]. \qquad \text{(B4)}$$

This relation is satisfied in three possible situations namely, the following.

1) The relaxation parameter $\beta = 0$. This, however contradicts the bounds on β, as given in (32).

2) The gradient $\psi(\hat{f}_l) = 0$. This solution corresponds to the unconstrained minimization of $\Phi(f)$. Obviously, the limiting solution $\hat{f}_l$ coincides with the Miller solution $\hat{f}_m$, defined in (29), and $\hat{f}_m$ satisfies the constraint C (i.e., $P\hat{f}_m = \hat{f}_m$). Hence, the Miller solution is consistent with the deterministic constraint C.

3) The gradient is not equal to zero for $\hat{f} = \hat{f}_l$. To satisfy the relation (B4), the projection operator P must exactly compensate the modifications in $\hat{f}_l$ in the direction $\psi(\hat{f}_l)$. Consequently, $\psi(\hat{f}_l)$ has to be orthogonal to the surface of the convex set C at the solution $\hat{f}_l$. By definition, $\psi(\hat{f}_l)$ is orthogonal to the surface of the set $\mathcal{K}$, defined by

$$\mathcal{K} = \left\{ h \,\middle|\, \Phi(h) \leq \Phi(\hat{f}_l) \right\}. \tag{B5}$$

Since (B5) defines a closed strictly convex set [19], and the constraint C a closed convex set, and the surfaces of these two sets are both orthogonal to $\psi(\hat{f}_l)$ at $\hat{f} = f_l$, we conclude that their intersection consists of exactly one element (namely, $\hat{f}_l$). Therefore, the functional $\Phi(f)$ attains its smallest value on the set C at the solution $\hat{f}_l$.

Hence, we have shown that the iteration (34) minimizes the functional $\Phi(f)$ subject to the (nonlinear) constraint C.

REFERENCES

[1] H. C. Andrews and B. R. Hunt, *Digital Image Restoration*. Englewood Cliffs, NJ: Prentice-Hall, 1977.

[2] J. Biemond, F. G. van der Putten, and J. W. Woods, "Identification and restoration of images with symmetric noncausal blurs," *IEEE Trans. Circuits Syst.*, vol. CAS-35, pp. 385-394, 1988.

[3] P. H. Westerink, J. Biemond, and P. H. L. de Bruin, "Digital color image restoration," in *Signal Processing III: Theories and Applications*, I. T. Young *et al.*, Eds. Amsterdam, The Netherlands: Elsevier North-Holland, 1986, pp. 761-764.

[4] J. W. Woods, J. Biemond, and A. M. Tekalp, "Boundary value problem in image restoration," in *Proc. IEEE Int. Conf. Acoust., Speech, Signal Processing 1985*, Tampa, FL, 1985, pp. 692-695.

[5] A. M. Tekalp, J. W. Woods, and H. Kaufman, "A multiple model algorithm for the adaptive restoration of images," in *Proc. IEEE Int. Conf. Acoust., Speech, Signal Processing 1983*, Boston, MA, 1983, pp. 832-835.

[6] R. C. Gonzalez and P. Wintz, *Digital Image Processing*. Reading, MA: Addison-Wesley, 1977.

[7] J. L. C. Sanz and T. S. Huang, "Unified Hilbert space approach to iterative least-squares linear signal restoration," *J. Opt. Soc. Amer.*, vol. 73, pp. 1455-1465, 1983.

[8] M. Bertero, C. de Mol, and C. A. Viano, "On the regularization of linear inverse problems in Fourier optics," in *Applied Inverse Problems*, Lecture Notes in Physics, vol. 85, P. C. Sabatier, Ed. Berlin: Springer-Verlag, 1978.

[9] M. Z. Nashed, "Operator-theoretic and computational approaches to ill-posed problems with applications to antenna theory," *IEEE Trans. Antennas Propagat.*, vol. AP-29, pp. 220-231, 1981.

[10] A. N. Tikhonov and V. Y. Arsenin, *Solutions of Ill-Posed Problems*. New York: Wiley, 1977.

[11] B. R. Hunt, "The application of constrained least-squares estimation to image restoration by digital computer," *IEEE Trans. Comput.*, vol. C-22, pp. 805-812, 1973.

[12] K. Miller, "Least squares methods for ill-posed problems with a prescribed bound," *SIAM J. Math., Anal.*, vol. 1, pp. 52-74, 1970.

[13] G. Wahba, "Practical approximate solutions to linear operator equations when the data are noisy," *SIAM J. Math. Anal.*, vol. 14, pp. 651-667, 1977.

[14] K. Stewart and T. S. Duranni, "Constrained signal reconstruction—A unified approach," in *Signal Processing III: Theories and Applications*, I. T. Young *et al.*, Eds. Amsterdam, The Netherlands: Elsevier North-Holland, 1986, pp. 1423-1426.

[15] R. W. Schafer, R. M. Mersereau, and M. A. Richards, "Constrained iterative restoration algorithms," *Proc. IEEE*, vol. 69, pp. 432-450, 1981.

[16] Y. Ichioka and N. Nakajima, "Iterative image restoration considering visibility," *J. Opt. Soc. Amer.*, vol. 71, pp. 983-988, 1981.

[17] H. J. Trussell, "Convergence criteria for iterative restoration methods," *IEEE Trans. Acoust., Speech, Signal Processing*, vol. ASSP-31, pp. 129-136, 1983.

[18] A. K. Katsaggelos and R. W. Schafer, "Iterative deconvolution using several different distorted versions of an unknown signal," in *Proc. IEEE Int. Conf. Acoust., Speech, Signal Processing 1983*, Boston, MA, 1983, pp. 659-662.

[19] D. C. Youla and H. Webb, "Image restoration by the method of convex projections: Part 1—Theory," *IEEE Trans. Med. Imaging*, vol. MI-1, pp. 81-94, 1982.

[20] H. J. Trussell and M. R. Civanlar, "The feasible solutions in signal restoration," *IEEE Trans. Acoust., Speech, Signal Processing*, vol. ASSP-32, pp. 201-212, 1984.

[21] M. I. Sezan and H. Stark, "Image restoration by the method of convex projections: Part 2—Applications," *IEEE Trans. Med. Imaging*, vol. MI-1, pp. 95-101, 1982.

[22] V. T. Tom, T. F. Quartieri, M. H. Hayes, and J. H. McClellan, "Convergence of iterative nonexpansive signal reconstruction algorithms," *IEEE Trans. Acoust., Speech, Signal Processing*, vol. ASSP-29, pp. 1052-1058, 1981.

[23] M. I. Sezan, A. M. Tekalp, and C. Chen, "Regularized signal restoration using the theory of the convex projections," in *Proc. IEEE Int. Conf. Acoust., Speech, Signal Processing 1987*, Dallas, TX, 1987, pp. 1565-1568.

[24] G. L. Anderson and A. N. Netravali, "Image restoration based on a subjective criterion," *IEEE Trans. Syst., Man, Cybern.*, vol. SMC-6, pp. 845-853, 1976.

[25] J. Biemond and R. L. Lagendijk, "Regularized iterative image restoration in a weighted Hilbert space," in *Proc. IEEE Int. Conf. Acoust., Speech, Signal Processing 1986*, Tokyo, Japan, 1986, pp. 1485-1488.

[26] R. L. Lagendijk, J. Biemond, and D. E. Boekee, "Iterative image restoration with ringing reduction," in *Signal Processing III: Theories and Applications*, I. T. Young *et al.*, Eds. Amsterdam, The Netherlands: Elsevier North-Holland, 1986, pp. 769-772.

[27] A. K. Katsaggelos, "Constrained iterative image restoration algorithms," Ph.D. dissertation, Georgia Inst. Technol., Atlanta, GA, Tech. Rep. DSPL-85-3, 1985.

[28] A. K. Katsaggelos, J. Biemond, R. M. Mersereau, and R. W. Schafer, "A general formulation of constrained iterative image restoration algorithms," in *Proc. IEEE Int. Conf. Acoust., Speech, Signal Processing 1985*, Tampa, FL, 1985, pp. 700-703.

[29] —, "Nonstationary iterative image restoration ," in *Proc. IEEE Int. Conf. Acoust., Speech, Signal Processing 1985*, Tampa, FL, 1985, pp. 696-699.

[30] A. K. Katsaggelos, "A general formulation of adaptive iterative image restoration algorithms," in *Proc. 1986 Conf. Informat. Sci. Syst.*, Princeton, NJ, 1986, pp. 42-46.

[31] H. J. Trussell and M. R. Civanlar, "The initial estimate in constrained iterative restoration," in *Proc. IEEE Int. Conf. Acoust., Speech, Signal Processing 1983*, Boston, MA, pp. 643-646.

[32] R. L. Lagendijk, R. M. Mersereau, and J. Biemond, "On increasing the convergence rate of regularized iterative image restoration algorithms," in *Proc. IEEE Int. Conf. Acoust., Speech, Signal Processing 1987*, Dallas, TX, 1987, pp. 1183-1186.

[33] M. R. Civanlar and H. J. Trussell, "Digital image restoration using fuzzy sets," *IEEE Trans. Acoust., Speech, Signal Processing*, vol. ASSP-34, pp. 919-936, 1986.

[34] J. Biemond and R. L. Lagendijk, "Digital restoration of noisy blurred images," in *Proc. 1st Euro. Conf. Imaging Visual Document. Med.*, in *Excerpta Medica*, K. Wamsteker *et al.*, Eds. Amsterdam, 1987, pp. 65-76.

[35] R. L. Lagendijk, A. K. Katsaggelos, and J. Biemond, "Iterative identification and restoration of images," in *Proc. IEEE Int. Conf. Acoust., Speech, Signal Processing 1988*, New York, 1988, pp. 992-995.

[36] L. M. Bregman, "The method of successive projection for finding a common point of convex sets," *Soviet Math. Doklady*, no. 6, pp. 688-692, 1965.

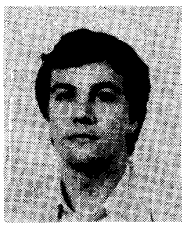

Reginald L. Lagendijk (S'87) was born in Leiden, The Netherlands, on April 22, 1962. He received the M.Sc. degree in electrical engineering from the Delft University of Technology, The Netherlands, in 1985.

Since 1985 he has been working toward the Ph.D. degree at the Information Theory Group of the Delft University of Technology. His research interests include information theory and multidimensional signal processing, with emphasis on image (sequence) identification and restoration, and image (sequence) coding.

Jan Biemond (M'80-SM'87) was born in De Kaag, The Netherlands, on March 27, 1947. He received the M.S. and Ph.D. degrees in electrical engineering from Delft University of Technology, Delft, The Netherlands, in 1973 and 1982, respectively.

He is currently an Associate Professor in the Laboratory for Information Theory of the Department of Electrical Engineering at the Delft University of Technology. His research interests include multidimensional signal processing, image enhancement and restoration, data compression of images, and motion estimation with applications in image coding and computer vision. He has authored and co-authored over 40 papers in these fields. In 1983 he was a Visiting Researcher at Rensselaer Polytechnic Institute, Troy, NY, and at the Georgia Institute of Technology, Atlanta.

Dr. Biemond is a member of the IEEE ASSP Technical Committee on Multidimensional Signal Processing. He served as the General Chairman of the Fifth ASSP/EURASIP Workshop on Multidimensional Signal Processing, held at Noordwijkerhout, The Netherlands, in September 1987.

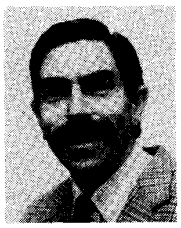

Dick E. Boekee was born in The Hague, The Netherlands, in 1943. He received the M.Sc. and Ph.D. degrees in electrical engineering in 1970 and 1977, respectively, from the Delft University of Technology, Delft, The Netherlands.

In 1981 he became a Professor of Information Theory at the Delft University of Technology. During 1979-1980 he was a Visiting Professor at the Department of Mathematics, Katholieke Universiteit Leuven, Heverlee, Belgium. His research interests include information theory, image coding, cryptology, and signal processing.